Proceedings of the 17th World Congress
The International Federation of Automatic Control
Seoul, Korea, July 6-11, 2008

Track-follow Control for High-density Probe-based Storage Devices

A. Pantazi, A. Sebastian, H. Pozidis, and E. Eleftheriou

IBM Zürich Research Laboratory, CH-8803 Rüschlikon, Switzerland

Abstract: Probe-based data-storage devices are being considered as ultra-high-density, small-form-factor and low-power alternatives to conventional data storage. Ultra-high storage densities of up to 1 Tb/in^2 or more can be achieved by using atomic force microscopy (AFM) techniques to write, read back, and erase data in very thin polymer films. High data rates are achieved by parallel operation of large arrays with thousands of micro/nanomechanical cantilevers. MEMS-based x/y micro-scanners are used to navigate the AFM probes over the storage medium. The ultra-high storage densities that probe-storage devices can realize pose a significant challenge to the control design for positioning and navigation. This paper focuses on the track-follow control of a MEMS-based micro-scanner for a high-density probe-based storage device. The positioning requirements are described, and controllers designed for tracking performance as well as controllers using sensor fusion are presented. Experimental results of information recorded at high densities and read back without errors validate the control performance.

1. INTRODUCTION

Ultra-high storage densities of 1 Tb/in^2 and beyond are the aim of the thermomechanical probe-storage concept presented in Vettiger et al. [2002] and Eleftheriou et al. [2003]. Digital information is stored as sequences of indentations written on thin polymer films using the tips of atomic force microscope (AFM) cantilevers, which are a few nanometers in diameter. The presence or absence of indentations corresponds to logical "1"s or "0"s, respectively. To increase the data rate, a 2D array of cantilevers is used, in which each cantilever performs write/read/erase operations in an individual storage field with an area on the order of approximately 100 μm $\times$ 100 μm.

In such systems, MEMS-based micro-scanners with 2D motion capabilities are used to position the storage medium with respect to the array of probes for parallel read/write operations (see Lantz et al. [2007]). Typical actuation distances are on the order of 100 μm. In addition to x/y actuators, global position sensors with a dynamic range of approx. 100 μm and displacement resolution of less than approximately 1 nm are required. Drift and low-frequency noise of global position sensing schemes will affect the performance of the control system in long-term operation of the device. Because multiple probes are available, a few probes and their storage fields could be dedicated for the generation of some form of medium-derived position-error signal (PES).

The ultra-high storage densities that probe-storage devices can realize pose a significant challenge to the control design for positioning and navigation. Nanometer-scale precision is required for a good error-rate performance at high densities. The positioning requirements for reliable recording performance at high densities are presented in this paper. Control designs that achieve high-accuracy tracking performance are presented. This is followed by the description of control architectures using sensor fusion motivated by the availability of two sources of position information. Experimental results obtained from a probe-based data-storage prototype validate the performance of the control architectures.

2. SYSTEM DESCRIPTION

The basis of the probe-based storage prototype is the MEMS assembly that consists of the cantilever-array chip, the micro-scanner and a silicon base-plate. The micro-scanner has x/y-motion capabilities that are on the order of the pitch between cantilevers in the array. To generate information on the position of the micro-scanner, two pairs of thermal position sensors are fabricated on the cantilever array chip. Alternative position error signal based on pre-written servo patterns on the medium can be used to obtain information on the micro-scanner position.

2.1 Micro-scanner

The micro-scanner is based on electromagnetic actuation and has x/y-displacement capabilities of about 120 μm, i.e., approximately 20% larger than the pitch between adjacent cantilevers in the array. The micro-scanner consists of a scan table, which carries the storage medium and two voice-coil-type actuators. Each voice-coil actuator consists of a pair of permanent magnets, with a miniature coil mounted between them on the base plate. Actuation in the x (y) direction is achieved by applying a current to the x (y) coil, which generates a force on the magnets and induces a displacement of the actuator. This motion is coupled to the scan table by means of a mass-balanced pivot scheme that translates the motion of the actuator to the scan table and also makes the micro-scanner robust against external shock and vibrations (see Lantz et al. [2007]).

A comprehensive model of the micro-scanner was developed for control design and simulation purposes (see Pan-

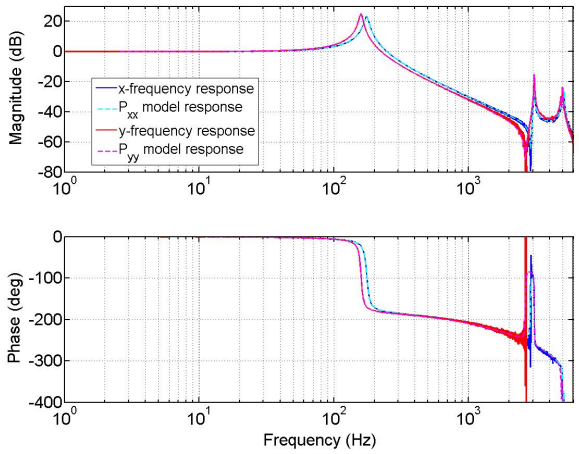

Fig. 1. Measured frequency responses of the micro-scanner in the x/y directions and the corresponding model responses.

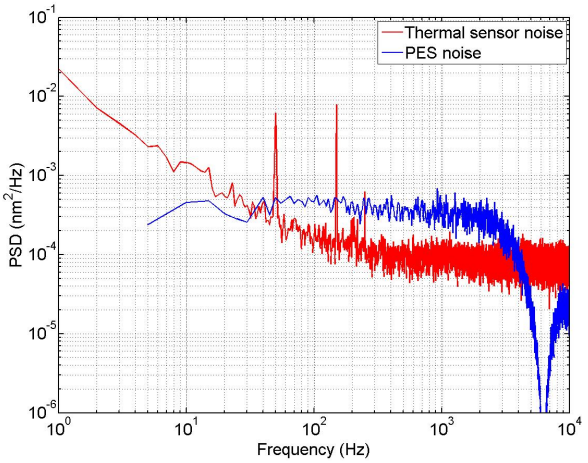

Fig. 2. Noise spectral characteristics of the thermal position sensors and the medium-derived PES.

tazi et al. [2007]). The motion of the micro-scanner in each direction is captured by the linear dynamic components, P_{xx} and P_{yy}. Specifically, the transfer function P_{xx} relates the coil current (u_x in mA) to the output displacement x (in μm), and the transfer function P_{yy} relates the coil current u_y to the output displacement y. To identify P_{xx} and P_{yy}, the frequency responses of the scanner in the x- and y-directions are obtained using the thermal position sensors. The experimentally obtained frequency responses in both directions and the corresponding model responses are shown in Fig. 1. As can be seen, the dynamics is dominated by the first mode, which can be accurately captured by a simple spring-mass-damper second-order model. In the higher-frequency regime, the micro-scanner frequency response exhibits higher-order resonance modes. It was also found that these higher-order resonances change as a function of the position on the x/y plane.

Another important characteristic that describes the motion of the micro-scanner is the cross-coupling between the axes. It was found that the cross-coupling is nonlinear and position-dependent (see Pantazi et al. [2007]). The cross-coupling on the y-axis due to x-motion exhibits a quadratic behavior as a function of the x-position.

2.2 Thermal position sensors

Two pairs of thermal position sensors are used to provide the x/y-position information of the micro-scanner (see Lantz et al. [2005]). These sensors are fabricated on the cantilever-array chip and positioned directly above the scan table. The sensors consist of thermally isolated, resistive strip heaters made from moderately doped silicon. Displacement of the scan table translates into a change in the temperature of these heaters and thus a change in their electrical resistance. By driving the sensors with a constant voltage, these changes in resistance can be detected by measuring the resulting current. To minimize drift effects, the sensors are operated in pairs using a differential configuration.

The behavior of the thermal-position sensors is important for the performance of the closed-loop system. Typically, a first-order response with a bandwidth of approx. 4 kHz accurately captures the differential sensor dynamics. The resolution of the thermal position sensor is approximately 1 nm over its sensing bandwidth. Even though the accuracy of the sensor is reasonably good, there is a significant low-frequency component, as can be seen from the power spectral density of the sensor noise shown in Fig 2. The predominant noise sources are Johnson noise and the $1/f$-noise of the silicon resistor.

2.3 Medium-derived position-error signal

The thermal position sensors can provide high-precision measurements of the micro-scanner position, but tend to suffer from low-frequency drift. An alternative medium-derived PES can be obtained by reading prewritten servo patterns on dedicated servo fields that are reserved exclusively for servo-control purposes. The approach for PES generation is based on the concept of vertically displaced bursts, arranged in such a way as to produce two signals in quadrature that guarantee a uniquely decodable PES, i.e., each PES value is mapped to a unique cross-track position (see Eleftheriou et al. [2003]). Therefore, the medium-derived PES accurately captures deviations from the track centerline for each data track.

Medium-derived PES can be generated using the servo burst configuration illustrated in Fig. 3. The A, B, C and D bursts are written in four different servo fields. Servo bursts labeled A and B are used to create the in-phase signal (I), and C and D the quadrature signal (Q). The cross-track distance between indentation centers of the same burst is equal to the track pitch (TP), whereas the distance between indentation centers in bursts A and B (or C and D) is TP/2. The distance between A and C is TP/4. The track centerlines of the data fields coincide with the centers of servo burst C.

For PES generation, a parallel read operation of the four servo fields is performed while scanning in the x-direction. The amplitude of the readback signal depends on the position of the tip relative to the recorded surface at the time of reading. The readback signal is strongest when the tip is positioned exactly over the center of a

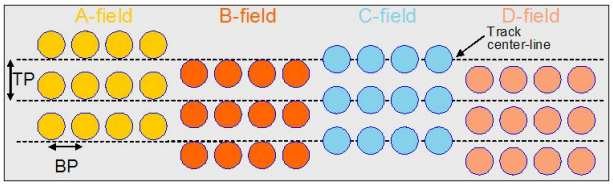

Fig. 3. Servo burst configuration.

written indentation. As the distance of the tip from the indentation center increases, the readout signal strength decreases, reaching a minimum level when the tip is away from the indentation. The in-phase signal is synthesized as the difference $\bar{B} - \bar{A}$ and the quadrature signal as the difference $\bar{D} - \bar{C}$, where the average bit depth values $\bar{A}$, $\bar{B}$, $\bar{C}$ and $\bar{D}$ correspond to bursts A, B, C and D, respectively. Note that the quadrature signal exhibits zero crossings at the points where the in-phase signal has local extrema. The final PES signal is generated by combining the two signals (I and Q), and has zero crossings at all track center locations, and an almost linear range between $-\mathrm{TP}/2$ and $\mathrm{TP}/2$. The medium-derived PES provides y-positional information around the track centerline, and therefore has a maximum range of TP. The medium-derived PES has a similar resolution as the thermal position sensor, but, unlike the thermal position sensor, provides good low-frequency fidelity as shown in Fig 2.

3. CONTROL SYSTEM

The servo control system in the MEMS-based storage prototype is responsible for writing the uniformly spaced data tracks and for reading them back with sufficient accuracy to guarantee a low error rate. As the areal density of such a system is increased to the Tbit/in^2 regime and beyond, the performance requirements for the servo system become very stringent. In general, the servo system in such a storage device has two functions. First, it locates the target track to which information is to be written or read back from, starting from an arbitrary initial position of the scan table carrying the storage medium. This is achieved by the seek-and-settle procedure. The second function of the servo system is to maintain the position of the read/write probes on the center of the target track while scanning along the length of this track. This is achieved by the track-follow procedure. During track-follow, each track is scanned in the horizontal direction with constant velocity, while maintaining the fine positioning in the cross-track direction in the presence of disturbances and noise. In the following sections we will describe the positioning requirements and control architectures that address these requirements for the track-follow procedure.

3.1 Positioning requirements

Probability of error is the key performance measure for a storage device. Primarily, the probability of error is determined by the signal-to-noise ratio (SNR) and the positioning inaccuracies. The SNR is mainly a function of the recording characteristics. On the other hand, the positioning inaccuracies due to the nanometer scale micro-scanner perturbations introduce distortions in the read-back signal. In this section, we will describe the positioning requirements for a high-density storage device for

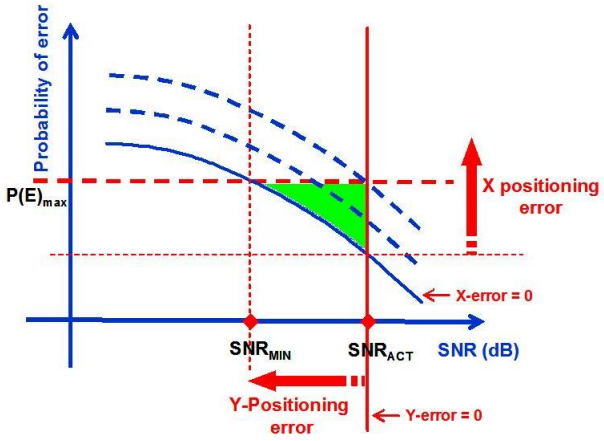

Fig. 4. Impact of positioning errors on device performance.

a given SNR available from the recording characteristics ($\mathrm{SNR}_{\mathrm{ACT}}$). In a 2D positioning system such as the micro-scanner described above, the positioning errors along both axes of motion influence the performance of the storage device. The influence of the x/y positioning errors on the performance of the storage device is described in Fig. 4, where the probability of error is plotted as a function of the SNR value. There is a marked difference between the ways in which the x- and y-positioning errors impact the system performance.

Specifically, the main objective of the control system in the y-direction is to maintain the position of the probes on the track centerline while writing and reading from the specific track. Deviations of the probes from the track centerline result in SNR loss in the readback signal. A reduced SNR naturally leads to an increased probability of error. Therefore, following the schematic description of Fig. 4 the increasing y-positioning error shifts the operating point on top of the curve to the left. On the other hand, the primary objective of the control system in the x-direction is to maintain a constant velocity while writing and reading information. The readback waveform is consequently processed by the read channel in order to detect the symbol information stored in each track. Simulations of the probe-based data-storage read channel show that there is a direct link between the x-positioning error and the probability of error for a fixed SNR (see Sebastian et al. [2007]). There is a steady increase in the probability of error as the x-positioning error increases. Therefore, in the diagram of Fig. 4 the increasing x-positioning error shifts the curve up (dashed curves). The maximum probability of error $P(E)_{\max}$ that is allowed by the error correction coding scheme used in the storage system defines the tolerable limits for the x/y-positioning error (shaded area). Thereafter, these limits define the positioning requirements for the track-follow procedure.

3.2 Control architectures for tracking performance

The primary objective of the track-follow controller is to maintain a constant velocity in the x-direction while keeping the position of the probes on the track centerline in the y-direction. This requirement can be translated to the ability of the closed-loop system to track the reference signal, to mitigate the effect of external shocks and vibra-

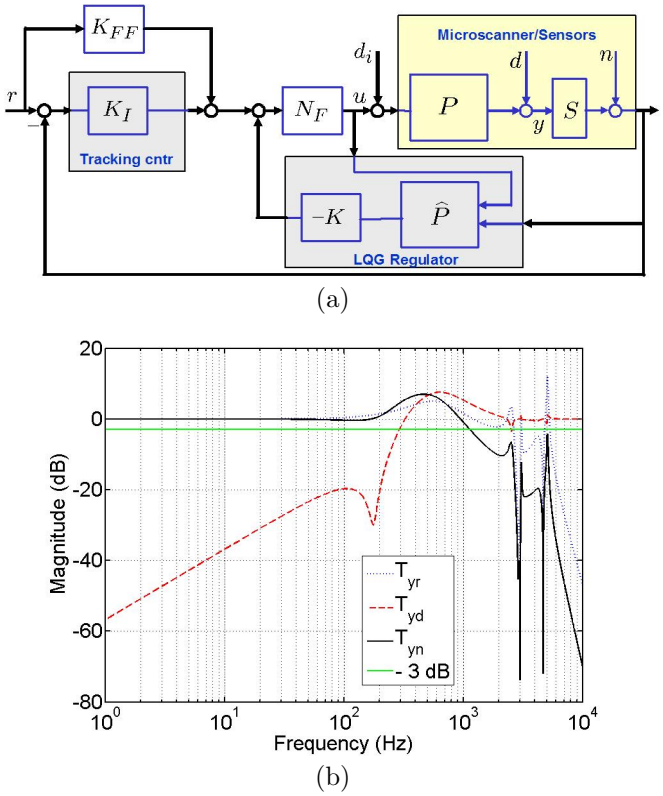

(a)

(b)

Fig. 5. (a) Block diagram and (b) closed-loop transfer functions for the LQG-based control architecture.

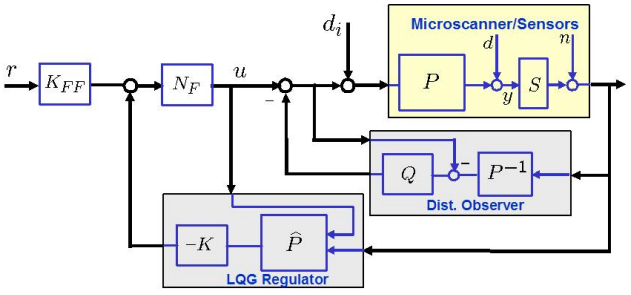

(a)

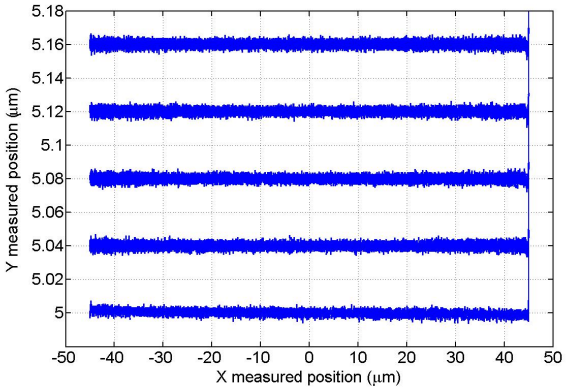

(b)

Fig. 6. (a) Block diagram and (b) track-follow performance for the control architecture based on disturbance observer.

tions and to reduce the effect of sensor noise on the position of the micro-scanner. A control architecture that is based on the position information of the global sensor is shown in Fig. 5(a). The controller for the x/y directions consists of an LQG regulator, a tracking controller, notch filters and a feed-forward component. In the block diagram of Fig. 5(a), P denotes the dynamics of motion of the micro-scanner in one direction and S represents the low-pass dynamics of the thermal sensor. Furthermore, r is the reference signal, y stands for the motion of the micro-scanner, and d_i, d, and n denote the input disturbance, the output disturbance and the noise signals, respectively. A set of notch filters, N_F, are incorporated into the feedback loop to minimize the effect of the higher-order resonances of the micro-scanner. The feed-forward component, K_{FF}, and the tracking controller, in this case an integrator K_I, are used for better tracking performance. A detailed analysis based on closed-loop transfer functions has been presented in Pantazi et al. [2007]. The closed-loop transfer functions T_{yr}, T_{yd}, and T_{yn} shown in Fig. 5(b) correspond to the x-direction and capture the performance of the feedback loop in terms of tracking, disturbance rejection and sensitivity to measurement noise, respectively. The reference tracking bandwidth of the system can be defined in terms of the -3 dB point of the transfer function T_{yr}. As shown in Fig. 5(b), a reference tracking bandwidth of more than 1 kHz has been achieved. Furthermore, from the high-pass shape of the T_{yd} transfer function, we can conclude that the system can adequately reject disturbances up to approximately 300 Hz. Using the noise sensitivity transfer function T_{yn} and the thermal sensor noise characteristics described in the previous section, the impact of measurement noise on the system can be estimated. The standard deviation of the estimated micro-scanner perturbation due to measurement noise was found to be approximately 0.65 nm. As mentioned earlier, the error rate performance of the storage device depends on the amount of timing jitter in the readback signal. Therefore, the accuracy of the thermal position sensors and the noise sensitivity characteristics of the closed-loop system are crucial for the reliability of the high-density storage system.

As the data rate per probe is relatively low, a linear scan velocity of a few millimeters per second would suffice for probe-based data storage. Hence the requirement on the tracking bandwidth is rather modest. However, disturbance rejection is of significant importance because of the external shocks and vibrations. In addition, in the y-direction, the feedback loop needs to mitigate the disturbances that originate from the cross-coupling in the y-position due to scanning motion in the x-direction. A control architecture that includes an inner loop with a disturbance observer is shown in Fig. 6(a). Disturbance observers have been proposed in the literature and are used to eliminate disturbances (see White et al. [2000] and Kempf et al. [1999]). In this architecture, the LQG controller described previously is used for tracking purposes and the integrator is removed because the integral action is assigned on the disturbance observer. The proposed control architecture allows independent tuning of the characteristics for reference tracking and for disturbance rejection. In addition, it could provide an improved transient response compared to integral control in the case of seek operations. The performance of the disturbance observer architecture is shown in Fig. 6(b), where the resulting x/y trajectory of the scan table for a typical

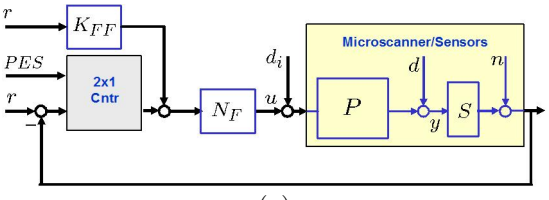

(a)

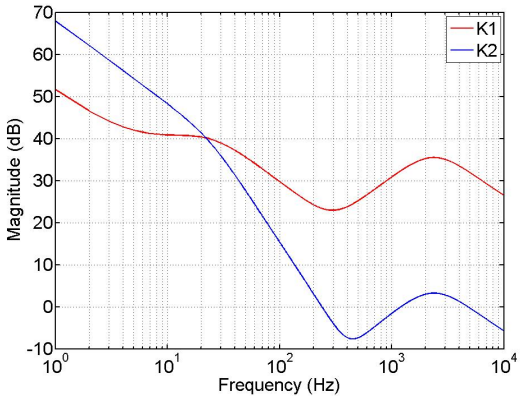

(b)

Fig. 7. (a) Block diagram and (b) controller transfer function for the H_∞ two-sensor control architecture.

track-follow procedure is presented. As shown in the figure, the disturbance observer-based control architecture has successfully rejected the effect of the cross-coupling in the y-position due to the x-motion.

3.3 Control architectures with sensor fusion

In a control scheme based solely on global-position sensor information, drift and low-frequency sensor noise may cause positioning errors. In the x-direction, the low frequency positioning errors are more tolerable since the read-back waveform is processed by the read channel where timing recovery circuits assist with the correction. On the contrary, in the y-direction errors originating from low-frequency noise can create deviations from the track centerline. Hence a feedback-control scheme relying on the global position sensors alone is not suitable for long-term operation of the device. Therefore, control architectures that have the capability of combining signals for different sensors are essential for reliable performance. In the case of probe-storage devices, medium-derived position information can be considered as a second sensor. A control configuration that employs both the global-position information from the thermal sensors and the medium-derived position information in a two-sensor-controller configuration is shown in Fig. 7(a) (see Pantazi et al. [2005]). The approach is based on the design of an H_∞ MISO optimal controller that takes into account the noise spectral characteristics of the two sensors. Therefore, with the *a priori* knowledge of the noise characteristics of both sensors, the controller can be designed such that the positional information from the medium-derived PES is primarily used for control at low frequencies. Using the H_∞ control framework, a controller that uses the best measurement in different frequency regions is designed. Figure 7(b) shows how the frequency separation is achieved from the transfer functions of the components of the resulting joint controller. The joint

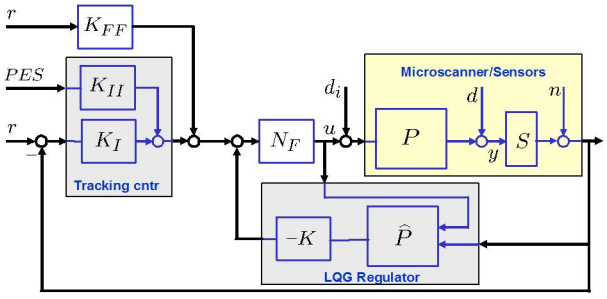

(a)

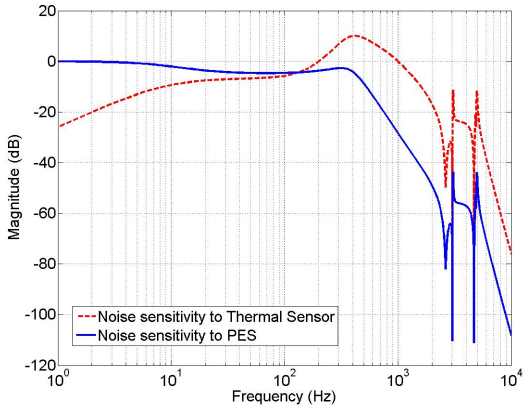

(b)

Fig. 8. (a) Block diagram and (b) noise sensitivity transfer functions for the sub-optimal two-sensor control architecture.

controller has a transfer function K_1 from the thermal-sensor error signal to the output and a transfer function K_2 from the PES to the output.

An alternate sub-optimal two-sensor scheme is illustrated in Fig. 8(a), where the estimation and the regulation are based only on the thermal sensor signal, as in the case of the controller presented in the previous section. The frequency separation in this scheme is assigned to the tracking controller, which is different for each of the sensors. Figure 8(b) shows the transfer functions that describe the impact of each of the sensors on the position of the micro-scanner. The final positioning error is a combination of the individual contributions of each sensor. Using the closed-loop transfer functions, the standard deviation of the micro-scanner positioning error due to the thermal sensor noise and the PES noise has been estimated to be 0.68 nm and 0.3 nm, respectively. Figure 9 shows the characterization of the y-positioning accuracy and the contribution of each sensor. The total y-positioning error has a standard deviation of 0.74 nm, which is expected to be within the tolerable limits.

4. READ/WRITE PERFORMANCE

A small-scale prototype system comprising all the critical components of a storage device has been built. The control system for the small-scale prototype consists of the controllers for the x/y directions. For this prototype demonstration, the control in the x-direction is based on the combination of an LQG and a tracking controller as presented above. For the y-direction, the sub-optimal

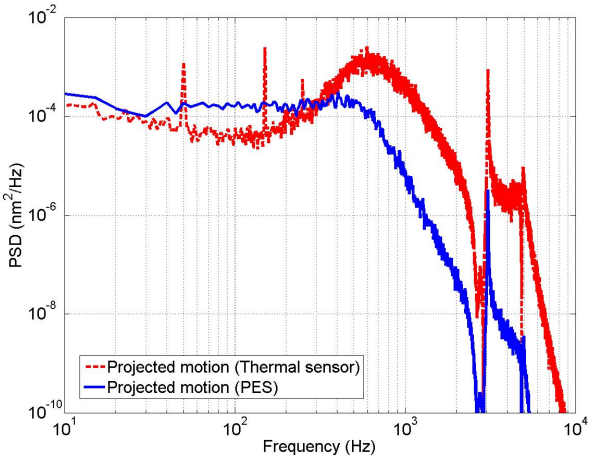

Fig. 9. Estimate of the y-positioning accuracy for the sub-optimal two-sensor control architecture.

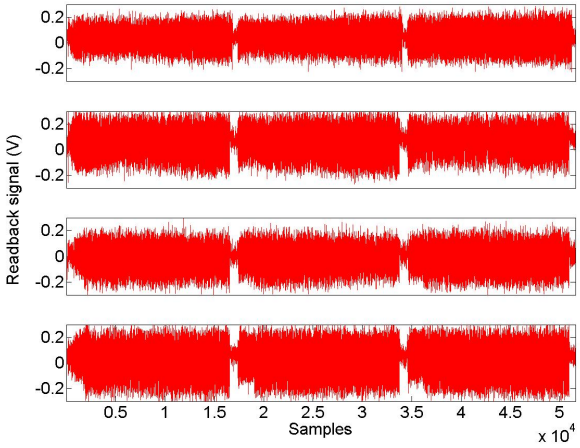

Fig. 10. Read-back signals from three different tracks using four cantilevers.

two-sensor scheme is employed. To further validate the positioning performance of the control system, parallel write/read operations are performed. Symbol sequences have been stored in four different data fields occupying three different data tracks in each field. The track size spanned 90 μm in the x-direction and the distance between adjacent tracks was 40 nm in the y-direction. The distance between adjacent symbols is 20 nm. The resulting areal storage density was 540 Gbit/in^2. Figure 10 shows the read-back signal from four cantilevers and three different tracks. Each row represents a different cantilever, and the three different tracks are shown as columns in the read-back signals. The readback signals from the levers were processed, and the symbols of each track were detected with a raw error rate of approx. 10^{-4}. This demonstration validates the positioning capability that is achieved. The control configuration has ensured convergence on the track centerline, accurate positioning during track-follow, and reliable stepping to the subsequent tracks.

5. CONCLUSION

Ultra-high storage densities beyond 1 Tb/in^2 can be achieved by probe-based storage technologies. The nano-scale positioning requirements for reliable recording performance were presented as well as different control approaches that achieve these requirements. Controllers for tracking performance and controllers using sensor fusion were described. Experimental results demonstrating the error-free recording and reading back of data at high densities validate the control performance.

ACKNOWLEDGEMENTS

We thank our colleagues of the Probe Storage Group at the IBM Zurich Research Laboratory. Special thanks go to M. Despont, U. Drechsler, M. Lantz, and H. Rothuizen for the design and fabrication of MEMS parts, to D. Jubin for the characterization and assembly of the MEMS components, and to P. Bächtold for the design of the electronics used in this work.

REFERENCES

E. Eleftheriou, T. Antonakopoulos, G. K. Binnig, G. Cherubini, M. Despont, A. Dholakia, U. Dürig, M. A. Lantz, H. Pozidis, H. E. Rothuizen, and P. Vettiger. Millipede-a MEMS based scanning-probe data storage system. *IEEE Trans. Magn.*, 39(2):938–945, 2003.

Carl J. Kempf and Seiichi Kobayashi. Disturbance Observer and Feedforward Design for a High-Speed Direct-Drive Positioning Table. *IEEE Trans. Control Syst. Technol.*, 7(5):513–526, 1999.

M. A. Lantz, G. K. Binnig, M. Despont, and U. Drechsler. A micromechanical thermal displacement sensor with nanometer resolution. *Nanotechnol.*, 16:1089–1094, 2005.

M. A. Lantz, H. E. Rothuizen, U. Drechsler, W. Häberle, and M. Despont. A vibration resistant nanopositioner for mobile parallel-probe storage applications. *J. Microelectromech. Syst.*, 16(1):130–139, 2007.

A. Pantazi, A. Sebastian, H. Pozidis, E. Eleftheriou. Two sensor based H_∞ control for probe storage in *Proceedings of IEEE Conference on Decision and Control*, pages 1174–1179, Dec. 2005.

A. Pantazi, A.Sebastian, G. Cherubini, M. Lantz, H. Pozidis, H. Rothuizen and E. Eleftheriou. Control of MEMS-based Scanning-probe Data Storage Device. *IEEE Trans. Control Syst. Technol.*, 15(5):824–841, Sept. 2007.

A. Sebastian, A. Pantazi and H. Pozidis. Jitter Investigation and Performance Evaluation of a Small-scale Probe Storage Device Prototype. In *Proceedings of the IEEE Global Telecommunications Conf*, pages 288–293, Nov. 2007.

P. Vettiger, G. Cross, M. Despont, U. Drechsler, U. Dürig, B. Gotsmann, W. Häberle, M. Lantz, H. Rothuizen, R. Stutz, and G. Binnig. The "millipede" - nanotechnology entering data storage. *IEEE Trans. Nanotechnol.*, 1(1):39–55, Mar. 2002.

M. T. White, M. Tomizuka, and C. Smith. Improved track following in magnetic disk drives using a disturbance observer. *IEEE/ASME Trans. Mechatron.*, 5(1):3–11, Mar. 2000.